Biomimetic Intelligence and Robotics 4 (2024) 100182

Contents lists available at ScienceDirect

Biomimetic Intelligence and Robotics

journal homepage: www.elsevier.com/locate/birob

Research Article

Design of a spider-inspired wheeled compliant leg for search mobile robots

Yilin Wang, Felix Pancheri, Tim C. Lueth, Yilun Sun *

Institute of Micro Technology and Medical Device Technology, Technical University of Munich, Garching 85748, Germany

ARTICLE INFO

Article history:
Received 7 May 2024
Revised 18 August 2024
Accepted 28 August 2024
Available online 6 September 2024

Keywords:
Compliant leg
Semi-tendon-driven mechanism
Biomimetic design
Search mobile robot

ABSTRACT

Earthquake and other disasters nowadays still threat people's lives and property due to their destructiveness and unpredictability. The past decades have seen the booming development of search and rescue robots due to their potential for increasing rescue capacity as well as reducing personnel safety risk at disaster sites. In this work, we propose a spider-inspired wheeled compliant leg to further improve the environmental adaptability of search mobile robots. Different from the traditional fully-actuated method with independent motor joint control, this leg employs an under-actuated compliant mechanism design with overall semi-tendon-driven control, which enables the passive and active terrain adaptation, system simplification and lightweight of the realized search robot. We have generalized the theoretical model and design methodology for this type of compliant leg, and implement it in a parametric program to improve the design efficiency. In addition, preliminary load capacity and leg-lifting experiments are carried out on a one-leg prototype to evaluate its mechanical performance. A four-legged robot platform is also fabricated for the locomotion tests. The preliminary experimental results have verified the feasibility of the proposed design methodology, and also show possibilities for improvements. In future work, structural optimization and stronger actuation elements should be introduced to further improve the mechanical performance of the fabricated wheeled leg mechanism and robot platform.

1. Introduction

Earthquake and other natural or man-made disasters are nowadays still great threats to human lives and property due to their destructiveness and unpredictability. Rescue time and sequence greatly affect survival rates of entrapped people. Most of the survivors are rescued within 2 days, and the average maximum survival time is around 6 days [1]. But paradoxically, first responders face the difficulties of irregular debris and destroyed road, risk their life in the aftershocks to race against time [2]. To address these problems, researchers are dedicated to developing post-disaster search and rescue (SAR) robots in order to enlarge team operation capacity and reduce personnel safety risk [3,4]. These robots are mainly divided into two major categories: unmanned ground and aerial vehicles (UGVs and UAVs). UAVs have unique advantages in mapping disaster areas, searching for exposed victims [5,6], and modeling damaged buildings [7], but is meanwhile limited in payload and cruise time.

The UGVs vary widely in shapes and sizes, and can be roughly divided into several types: wheeled, legged, tracked, snake-like, etc. "Quince" is a well-developed tracked vehicle platform with four rotatable sub-tracks, which allow adjusting to environment and climbing over obstacles [8,9], but has limitations in handling side tumbling. Boston Dynamics has launched many legged dog-like robots since "BigDog" in 2008 [10], all the way to the latest "Spot" [11]. They have impressive dynamic adjustment capabilities and a certain terrain adaptability and payload capacity, at the cost of an extremely high price. Some recent works such as "Toqro" and "TurBot" uses topology optimized soft or soft-rigid hybrid legs to achieve a balance between load capacity and environmental adaptability with simplified mechanisms [12–14]. Snake-like robots can travel through narrow spaces and enter collapsed buildings to search for trapped targets [15–17]. In addition, worm robots have been a research hot spot in recent years. They are soft robots with pneumatic, electric or other types of retractable actuators. Some inchworm-inspired robots can carry load several times of itself, and has the advantage of self-sensing of posture [18], while some can transport objects within cavities to reach curved and narrow spaces [19,20].

Each type of locomotion system has its inherent strengths and drawbacks, combinations of two or even more types of mechanisms are thus also common. The Institute of Intelligent Systems and Robotics (ISIR) of Sorbonne University have designed several wheel-legged robots as well as control algorithms since "Hylos" in 2000, which are driven forward by the wheels on the end

* Corresponding author.
E-mail address: yilun.sun@tum.de (Y. Sun).

https://doi.org/10.1016/j.birob.2024.100182

of leg, and can change posture to cross obstacles through control of the four legs [21–24]. In the later version "Complios", compliant components are integrated on purpose of improving ground adaptation ability [25,26]. Some other designs also try to take advantage of both wheels and legs to achieve high velocity and flexibility at the same time, for example the "wheel-on-leg" type of "Epi.q-1" [27], "ANYmal" [28], "BIT-6NAZA" [29], and the "wheel-to-leg" (transform) type of "Quattroped" [30], "Wheel Transformer" [31] and some unnamed designs [32].

Although a lot of robot designs have been proposed and tested in laboratory or field, the current state of the art still leaves much to be improved [33,34]. For example, rigid-leg robots usually need to go through a series of processes of perception, calculation and control to achieve the ability to move on complex terrain [35,36]. This is accompanied by a large number of sensors and actuators, as well as heavy body, costly production, and complex and time-consuming control networks [37]. Even in the field of soft robots, too much flexibility in the locomotion system can lead to insufficient traction force, speed, and load capacity [38,39]. Moreover, many SAR robots are not easy to use and only operated by developers themselves, but not the responders [40]. These shortcomings hinder their large-scale use in search and rescue scenarios. Especially with limited transportation capacity in the immediate aftermath of a disaster, they were not efficient enough to be brought to the scene.

Therefore, in this work, we propose a wheeled compliant leg with a spider-inspired mechanism design to improve the environmental adaptability of search mobile robots (Fig. 1). Different from the traditional fully-actuated control strategy, we have incorporated three compliant joints into the leg design to maintain the nominal configuration and enable passive adaptation of the leg to uneven grounds. In addition to the passive adaptation mode, a leg-lifting mode is also introduced to allow the leg to actively climb over higher obstacles. Accordingly, two motors are integrated into the leg for actuation, where one motor is used to drive the wheel forward, and the other is used to lift the leg up with a tendon-driven mechanism. The potential advantages of the proposed design are simple-yet-efficient structure, light weight and adaptability to the environment.

The main contributions of this paper are concluded as below:

- Conceptual design of a spider-inspired semi-tendon-driven wheeled leg for search mobile robots to achieve both passive and active obstacle-crossing.
- A generalized theoretical model and a program-assisted design method for the proposed wheeled compliant leg.
- Preliminary evaluation of the design concept by performing experiments on a one-leg prototype and a four-legged robot platform.

The rest of the article is organized as follows. The concept of the leg and robot design is described in Section 2. The theoretical analysis, the scheme of the analysis program as well as design procedure and results are presented in Section 3. A specific design of the leg is depicted in Section 4. In Section 5, the fabricated prototypes and the corresponding experiments are presented. Finally, Section 6 concludes the article and indicates the prospect.

2. Concept and working principle

2.1. Working principle of the robot

Fig. 2 shows the conceptual structure of the proposed spider-inspired wheel-legged robot. Different from a normal "dog-like" quadruped robot, which places its legs under the body and moves them mostly parallel to the sagittal plane, this "spider-like" robot distributes its legs diagonally, and stretches its upper leg above the chassis plane. Compared to a conventional fully-actuated legged robot with similar leg length, this spider-like wheel-legged robot distributes more weight on the wheels that are in direct contact with the ground, and the chassis is relatively low. This results in a lower center of gravity (COG). In addition, the diagonally extended legs have created a wide, nearly square support area. Based on these features, the proposed robot can efficiently avoid rollover during locomotion.

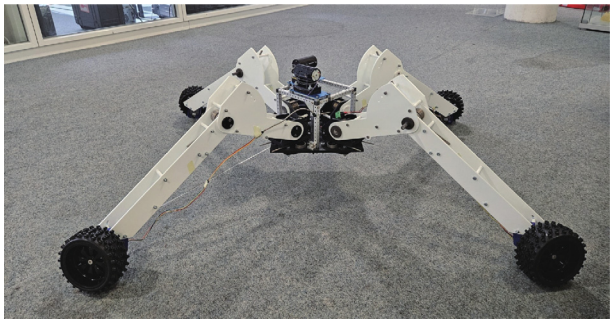

Fig. 1. A robot platform with the proposed spider-inspired wheeled compliant legs.

This robot has two operation modes:

I. **Driving and passive adaptation**. In this mode, the wheels rotate under the direct drive of the motors to drive the robot forward. The leg configuration will not be actively manipulated at this stage. With the introduced compliant joints, the legs can passively adapt to uneven ground and work as independent suspensions for each wheel, making the mobile robot move like an off-road vehicle.

II. **Leg-lifting**. When robot encounters an obstacle that cannot be overcome by the passive mode, it switches to the leg-lifting mode. In this case, the legs are lifted one by one through active tendon-pulling to climb over the obstacle. The wheels also help to drive forward in this process.

Different from other mobile robots that actively adapt to obstacles, the proposed robot mainly works in the passive mode, and the obstacle-crossing performance is achieved by the compliance and flexibility of the legs. In addition, due to the effect of inertia, a higher running speed can also improve the passive obstacle-crossing ability.

2.2. Design concept of the compliant leg

Each leg has three degrees of freedom to adjust its configuration, and another DOF for the wheel on the end of the leg to drive forward. As Fig. 3 shows, the yaw joint allows the leg to rotate about a vertical axis to change its orientation. The pitch and fold joints are parallel, enabling the leg to be raised and folded. With these three revolute joints, the wheel on leg can reach any position within range and well adapt to the irregular terrain.

These joints would be kept around so-called nominal joint angles by compliant elements (represented in orange in Fig. 3), such as torsional springs, which are placed in the joints with chosen initial installation angles. When a disturbance acts on the wheel, the configuration of the leg is slightly changed, restoring torques are subsequently generated by compliant elements, which tend to push the links back to where they were and recover the nominal configuration.

A wheel motor is mounted in the ankle and fixed on the end of each leg, and a rubber off-road wheel is connected to the wheel motor through a coupling. Due to the diagonal leg orientation, there is an offset angle between the wheel plane and the leg

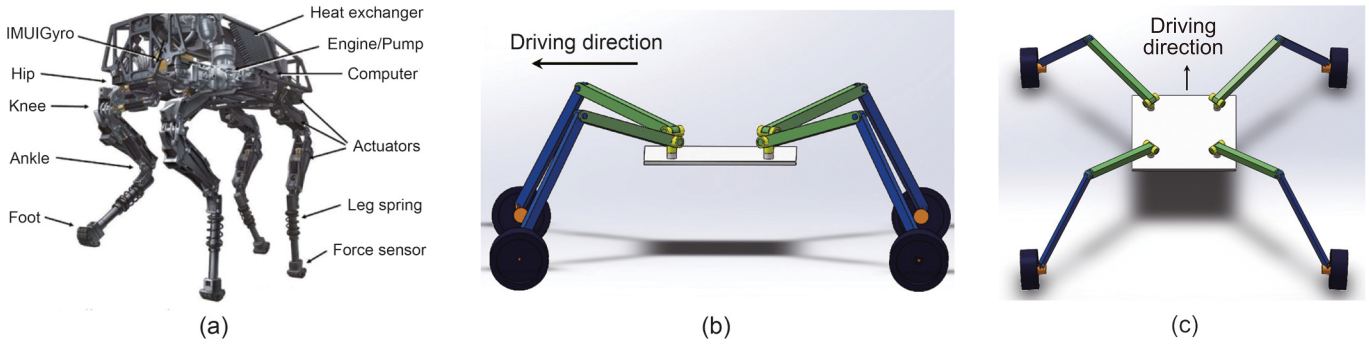

Fig. 2. Comparison of the proposed spider-inspired wheel-legged robot and the conventional quadruped robot. (a) The structure of BigDog, a conventional fully-actuated quadruped robot with vertical legs [10]. (b) The conceptual structure of the spider-inspired wheel-legged robot with diagonal leg configuration and low COG (from side view). (c) The spider-inspired wheel-legged robot from upper rear view.

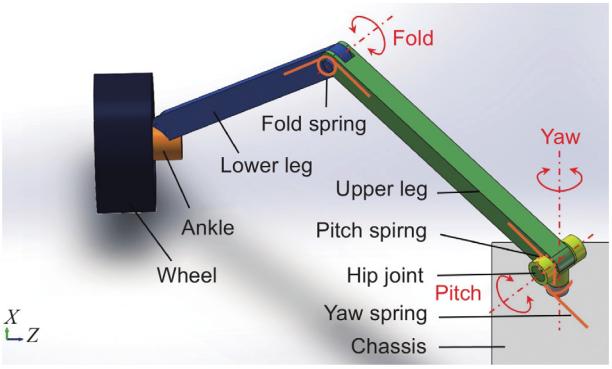

Fig. 3. Conceptual leg structure. Yaw, pitch and fold are three rotational degrees of freedom of the leg.

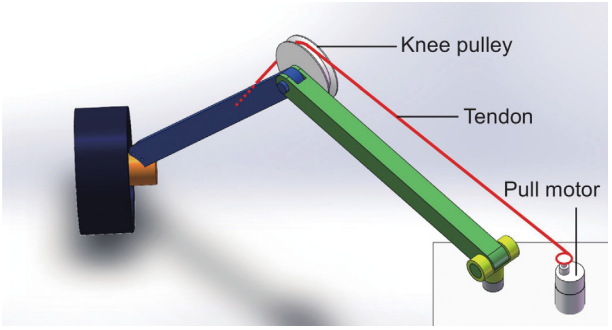

Fig. 4. Conceptual structure of the leg-lifting Mechanism.

plane, making the wheel plane roughly parallel to the travel direction. Energy supply and control module for wheel motors will be bound on chassis.

If a leg-lifting action is required, the tendon is dragged by pull motor to raise the whole leg (Fig. 4). All the three leg joints are controlled by a single tendon simultaneously, which means it is a semi-tendon-driven mechanism, whose number of actuators is less than the joint DOFs [41]. Under the action of the same tendon force, the rotation angle of each joint will be distributed according to the lengths of the moment arms and resistances, just like series resistors distribute the voltage according to their respective resistance values. By reasonably selecting parameters, we can pre-design the trajectory that the wheels will pass during the leg-lifting process totally though mechanism design, instead of using multi-motor collaborative control like a general robot.

In addition to simplifying the structure and reducing the number of motors, another advantage of this design is that the configuration can be self-adapted to obstacles. In this case, the joint angles are automatically redistributed, the wheel begins to move along the surface of the obstacle, and the leg-lifting action continues.

3. Theoretical analysis and program

In this section we conduct force analysis of the leg for parameter design and then implement the resulting equations in a MATLAB program. With the help of program-assisted computation and visualization, we can intuitively observe the effect of changing parameters and find a proper parameter set, so that the robot can travel stably and have adequate stiffness as well as flexibility to resist interference caused by obstacles. In addition, an appropriate end trajectory while leg-lifting is also desired.

3.1. Theoretical analysis

3.1.1. State I: Driving

Assume that the robot is placed on flat ground without preload between its four legs, the robot is symmetrical and all legs have same configuration. Therefore, the support and friction forces of the ground facing the wheel is equally distributed.

$$N = (m_w + m_t + m_f + \frac{1}{4}m_c)g \tag{1}$$

The moment balance equation of the leg around yaw axis is:

$$\tau_{yaw} = f_\tau(l_t cos(\theta_t - \theta_f) + l_f cos\theta_f) \tag{2}$$

where f_r and f_τ are friction forces along and perpendicular to the leg plane respectively (Fig. 5). l_f and l_t are the lengths of the upper leg (here called femur) and lower leg (tibia). θ_f and θ_t are the joint angles of pitch and fold joints (Fig. 6).

Similar, balance equations around pitch and fold axis are given by

$$\begin{aligned}\tau_{pitch} =&((1-c_t)m_t + m_f + \frac{1}{4}m_c)gl_t cos(\theta_t - \theta_f)\\ &+ ((1-c_f)m_f + \frac{1}{4}m_c)gl_f cos\theta_f\\ &+ f_r(R_w + l_t sin(\theta_t - \theta_f) - l_f sin\theta_f)\end{aligned} \tag{3}$$

$$\begin{aligned}\tau_{fold} =&((1-c_t)m_t + m_f + \frac{1}{4}m_c)gl_t cos(\theta_t - \theta_f)\\ &+ f_r(R_w + l_t sin(\theta_t - \theta_f))\end{aligned} \tag{4}$$

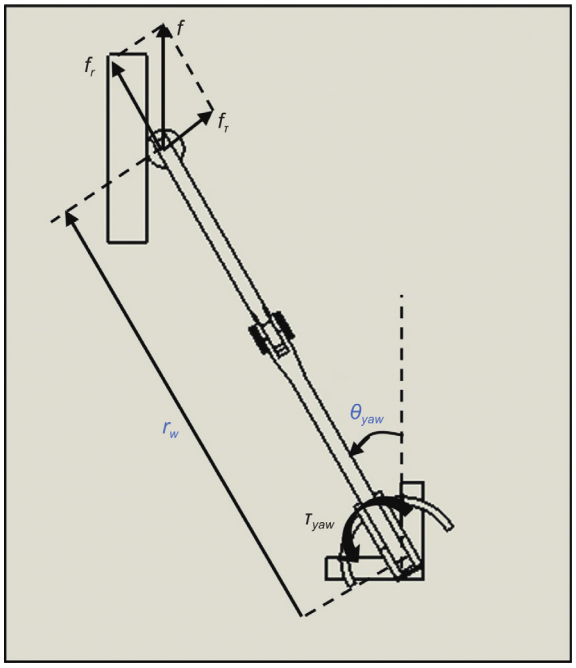

Fig. 5. Force analysis diagram of the leg in driving state I from top view.

where c_f and c_t mark the ratio of the distance from the femur (or tibia) COG to the pitch (or fold) joint axis to the length of the link. m_c, m_f, m_t and m_w are respectively the mass of chassis (and the whole robot body), femur, tibia and wheel (together with ankle, wheel motor etc.)

The right side of the formula includes the effects of gravity forces and ground friction. The left side is joint torque required to balance the external forces, which is provided completely by compliant joint in passive adapting state I. In this work, torsional springs are utilized and assumed to be linear.

$$\tau_{yaw} = k_{yaw}(\theta_{0yaw} - \theta_{yaw}) \tag{5}$$

$$\tau_{pitch} = k_{pitch}(\theta_f - \theta_{0f}) \tag{6}$$

$$\tau_{fold} = k_{fold}(\theta_{0t} - \theta_t) \tag{7}$$

where k is the torsional stiffness of the torsional spring, θ_0 represents the joint angle where the torsional spring provides no elastic force, which is also called the installation angle in this paper.

With Eqs. (2)–(7), in one hand, we can determine the equilibrium configuration $(\theta_{yaw}, \theta_f, \theta_t)$ with a given robot structure, spring parameters and friction forces. In the other hand, we can also apply a desired equilibrium to the equations on purpose of spring design.

3.1.2. State II: Leg-lifting

A static force analysis is performed to figure out the relationship between tendon pulling force and the leg configuration during free leg-lifting. "Free" means the wheel does not come into contact with obstacles in the process.

The main differences between the free leg-lifting state and the driving state are: 1. there are no longer support or friction forces of the ground on the wheel while lifting. 2. Tendon force provides joint torques and works against spring torques as well as gravity.

The balance equations of the three joints are thus:

$$\tau_{Tyaw} = k_{yaw}(\theta_{0yaw} - \theta_{yaw}) \tag{8}$$

$$\begin{aligned}\tau_{Tpitch} =& k_{pitch}(\theta_f - \theta_{0f}) \\ &+ m_w g(l_t cos(\theta_t - \theta_f) + l_f cos\theta_f) \\ &+ m_t g(c_t l_t cos(\theta_t - \theta_f) + l_f cos\theta_f) \\ &+ m_f g c_f l_f cos\theta_f\end{aligned} \tag{9}$$

$$\begin{aligned}\tau_{Tfold} =& k_{fold}(\theta_{0t} - \theta_t) \\ &+ m_w g l_t cos(\theta_t - \theta_f) \\ &+ m_t g c_t l_t cos(\theta_t - \theta_f)\end{aligned} \tag{10}$$

The joint torque brought by the tendon is the product of the pulling force and the moment arm, but in this mechanism, the moment arm for each joint axis changes with the joint angles. As shown in Figs. 7 and 8, we mark the coordinates of the starting point of the tendon as (x_p, y_p, z_p) and its projected coordinates on the leg plane as (r_p, z_p). The tangent point between the rope and the pulley is labeled as (x_k, y_k, z_k). The orientations of the projections of the tendon perpendicular to the yaw and pitch axis are named as θ_{Ty} and θ_{Tp} respectively. Expressions for coordinates are given based on geometric relationships.

$$r_p = -y_p cos\theta_{yaw} + x_p sin\theta_{yaw} \tag{11}$$

$$\begin{aligned}\theta_{Tp} =& arctan(\frac{l_f sin\theta_f - z_p}{l_f cos\theta_f + r_p}) \\ &+ arcsin(\frac{R_k}{\sqrt{(l_f sin\theta_f - z_p)^2 + (l_f cos\theta_f + r_p)^2}})\end{aligned} \tag{12}$$

$$x_k = -(l_f cos\theta_f - R_k sin\theta_{Tp}) sin\theta_{yaw} + S_k cos\theta_{yaw} \tag{13}$$

$$y_k = (l_f cos\theta_f - R_k sin\theta_{Tp}) cos\theta_{yaw} + S_k sin\theta_{yaw} \tag{14}$$

$$z_k = l_f sin\theta_f + R_k cos\theta_{Tp} \tag{15}$$

$$\theta_{Ty} = arctan(\frac{y_k - y_p}{-x_k + x_p}) \tag{16}$$

where R_k and S_k are the radius and offset of the knee pulley.

Then we can calculate the projections of tendon force as well as the joint torques:

$$T_y = T \cdot \frac{\sqrt{(x_k - x_p)^2 + (y_k - y_p)^2}}{\sqrt{(x_k - x_p)^2 + (y_k - y_p)^2 + (z_k - z_p)^2}} \tag{17}$$

$$\tau_{Tyaw} = T_y(x_p sin\theta_{Ty} + y_p cos\theta_{Ty}) \tag{18}$$

$$T_p = T \cdot \frac{\sqrt{(l_f cos\theta_f - R_k sin\theta_{Tp} + r_p)^2 + (l_f sin\theta_f + R_k cos\theta_{Tp} - z_p)^2}}{\sqrt{(x_k - x_p)^2 + (y_k - y_p)^2 + (z_k - z_p)^2}} \tag{19}$$

$$\tau_{Tpitch} = T_p(r_p sin\theta_{Tp} + z_p cos\theta_{Tp}) \tag{20}$$

$$\tau_{Tfold} = T \cdot R_k \tag{21}$$

Substituting the joint torques into balance equations, the leg configuration $(\theta_{yaw}, \theta_f, \theta_t)$ can be solved with a certain given tendon force T. Considering the joint angles limits as well, we can draw the leg-lifting end trajectory by selecting a series of pulling forces. Unlike ordinary robots, this end trajectory is predefined by the mechanism characteristics, or occasionally self-adapted to obstacles. Adjusting the pulling force can only control the position of the leg end on this trajectory.

From another perspective, it is easy to use. All the operator needs to do is "press the leg lift button", wait for the leg to cross the obstacle by itself, and then "press the leg release button" to release the tendon and let the leg stand on the step under the effort of gravity and spring forces and pull the robot body upwards.

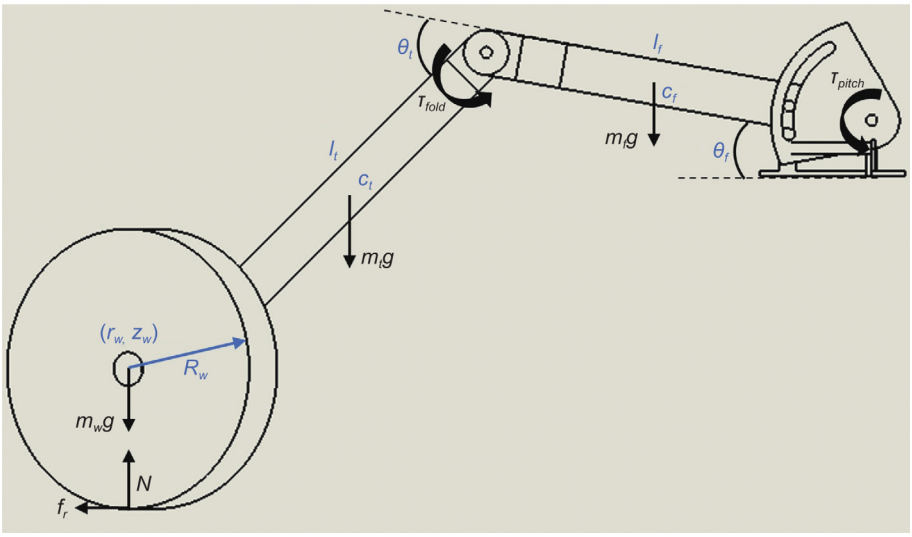

Fig. 6. Force analysis diagram in driving state I from side view of the leg.

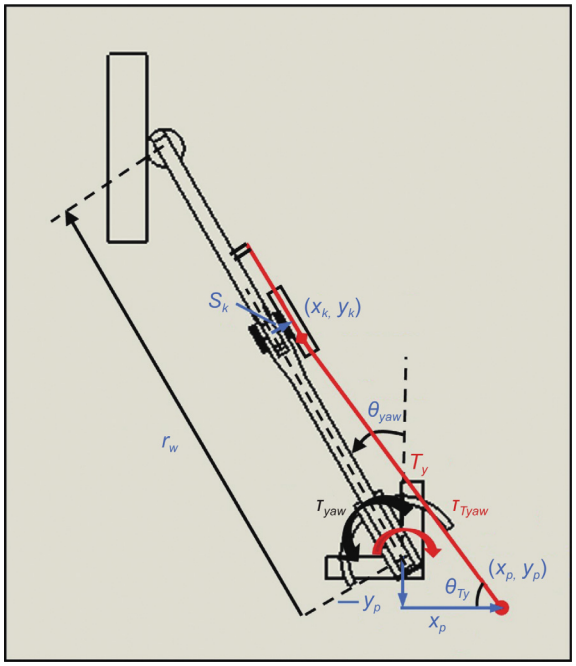

Fig. 7. Force analysis diagram of the leg in leg-lifting state II from top view.

3.2. Program-assisted parameter design

Since there are a lot of parameters that affect the mechanism's behavior, we developed a MATLAB program to calculate and visualize the end trajectory under different parameters. This program is used to analyze the impact of different parameters on the trajectory and select an appropriate set of parameters.

The program structure is shown in Fig. 9. In the program, all relevant parameters of the leg are first initialized, and can be easily modified during the design process. They are defined as global variables, so that they can be accessed in functions as well as in sections in main script. The visualization programs to assist design and the commands to adjust parameters are arranged in the sections of the main function. Equations in Section 3 are encapsulated in the form of functions.

In response to different design needs, we propose two different design processes separately for the driving state (state I) and leg-lifting state (state II).

In the driving state, the design objects are the stiffness k and installation angles θ_0 of torsional springs that are integrated in the leg joints. Taking the design of pitch torsional spring as an example, the procedure is as follows:

(1) Initialize leg parameters, including desired nominal joint angles of the three joints.
(2) Draw the required joint torque as a function of pitch angle (the right-hand side of Eq. (3)), supposing that the other angles do not change (red curve in Fig. 10(a)).
(3) Design a compliant element characteristic curve that meets the need (Eq. (6)). Here we utilize linear torsional spring, whose characteristic curve is a straight line in this τ_{pitch} - θ_f diagram (the purple straight line in Fig. 10(b) - (d)).
(4) Summarize the design parameters (k_{pitch} and θ_{0f}) from the characteristic curves.

The intersection point of the required torque and spring torque curves is exactly the equilibrium angle of the joint. The slop of the purple straight line represents the torsional stiffness of the spring k_{pitch}, and the X-intercept is the installation angle θ_{0f}, where the spring provides no torque. The equilibrium configuration of the leg is stable under instant disturbance, and shiftable under variable loads. On one hand, if the wheel encounters a small stone, it is subjected to a short impulse and a rapid change of the leg's end position occurs, resulting in a change of joint angles (such as $\Delta\theta_f$ in Fig. 10(c)). Under the condition that the slop of the purple curve (spring-provided joint torque) is larger than the red curve (required joint torque for balancing) around the equilibrium point, a restoring force $\Delta\tau$ is generated and pushes the femur back to its equilibrium angle after the disturbance faded. On the other hand, when the robot accelerates or decelerates, an additional friction force f_r is provided by ground to the wheel. In this circumstance, the curve of required joint torque is shifted to the yellow or blue curves in Fig. 10 and the equilibrium points changes accordingly. Similar passive adaptations to dynamic stresses happen on yaw and fold joints as well.

We should consider three main aspects while designing the compliant element characteristic curve: (i) Equilibrium position. It defines the nominal configuration of the leg, therefore decides the robot chassis height and wheel track. (ii) Joint stiffness. Different from the spring stiffness, the joint stiffness describes the

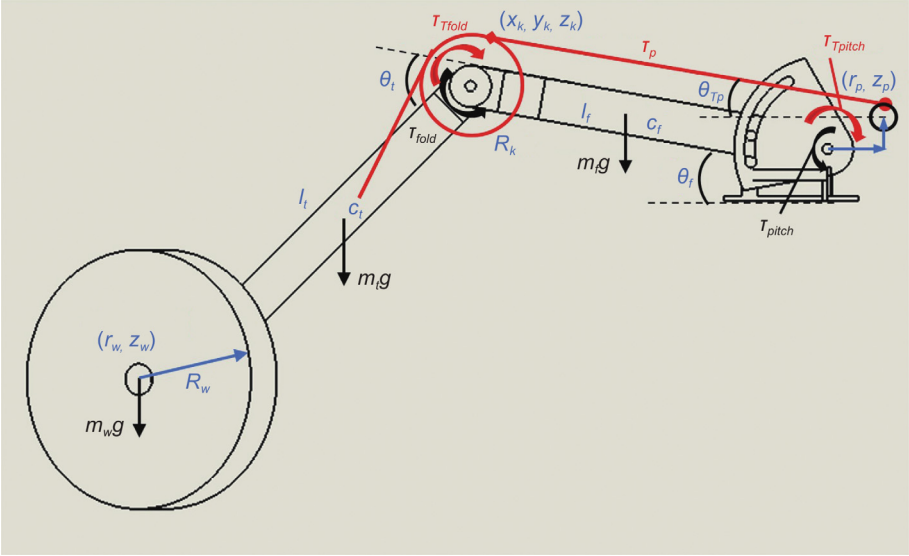

Fig. 8. Force analysis diagram of the leg in leg-lifting state II from side view.

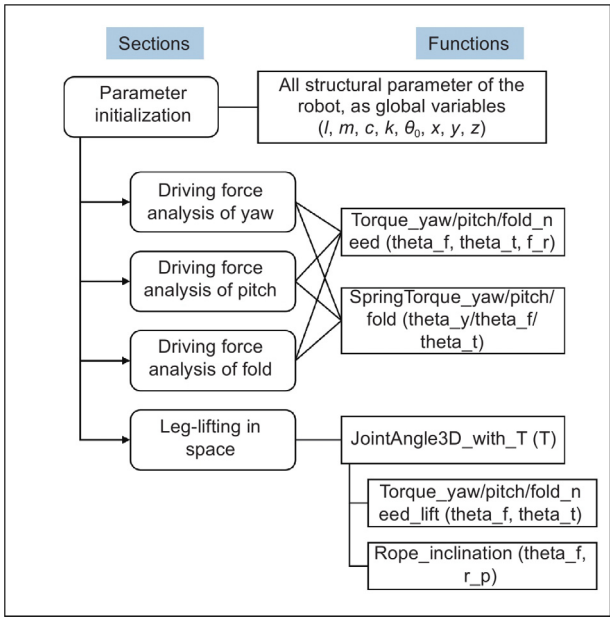

Fig. 9. Structure of the analysis and design assistant program.

ability of the joint to recover from perturbations. It can be visually observed in Fig. 10(c), $\Delta\tau$ is the difference between spring torque and required torque, i.e., the restoring torque, under a disturbance $\Delta\theta$ from the equilibrium. An appropriate joint stiffness not only ensures the maintenance of the robot's configuration during travel, but also allows flexible obstacle avoidance capabilities. (iii) Resistance during lifting. During the leg lifting process, the joint angle is greatly moved away from the equilibrium point, and a linear spring with high stiffness will cause great resistance at this time. Fig. 10(d) shows design variants of the compliant element, and the resistance can be reduced by using nonlinear elements (green line) or reducing the spring stiffness (light blue line). When using nonlinear compliant elements, Eq. (5)–(7) should be replaced by corresponding characteristic formulae.

This intuitive, visual design process works well for all kinds of compliant elements and can aid future work.

In the leg-lifting state, design parameters are radius of knee pulley R_k and the coordinates of tendon starting point (x_p, y_p, z_p). We change one of the parameters individually and observe its impact on the end trajectory.

The relationships of three joint angles with respect to tendon pulling force (Fig. 11) as well as the end trajectory in space (Fig. 12) are visualized with the help of our MATLAB analysis program.

Parameters for the blue reference curve are $R_k = 0.035$ m, $(x_p, y_p, z_p) = (0.01, -0.01, 0.1)$ m. Under this setting, pitch joint is the most sensitive to tendon force. The wheel is first raised thanks to the rapid increase of pitch angle and the "week knee", and then move forwards and toward the middle as yaw and fold joints rotate.

The red curves represent the situation where the tendon starting point is set further away horizontally, $(x_p, y_p, z_p) = (0.02, -0.02, 0.1)$ m, so that the tendon force has a larger moment arm with respect to yaw axis. With this adjustment, the yaw joint is now more vulnerable and yaw angle decreases much more rapidly compared to the reference. Reflected in the trajectory, the impact is that the wheel moves further horizontally in the early stage before being lifted high enough. This can make it easier to hit the side of an obstacle rather than cross it from above.

If we replace the knee pulley with a larger one, the resulting change is shown in the pink curve. The fold joint become "softer", and the raising of the lower leg and the rotation of yaw joint are synchronized. The most forward point is reached on the half way, not after the leg is fully extended straight ahead, and is higher than reference. The biggest advantage of a large knee pulley is that less tendon force is required to reach the furthest point. However, whether this farthest point is suitable still needs to be considered.

In summary, above we have proposed the theory and parameter design method for both states of the three-degree-of-freedom compliant leg driven by a single tendon. These achievements can also be generalized to other similar mechanisms after slight modification.

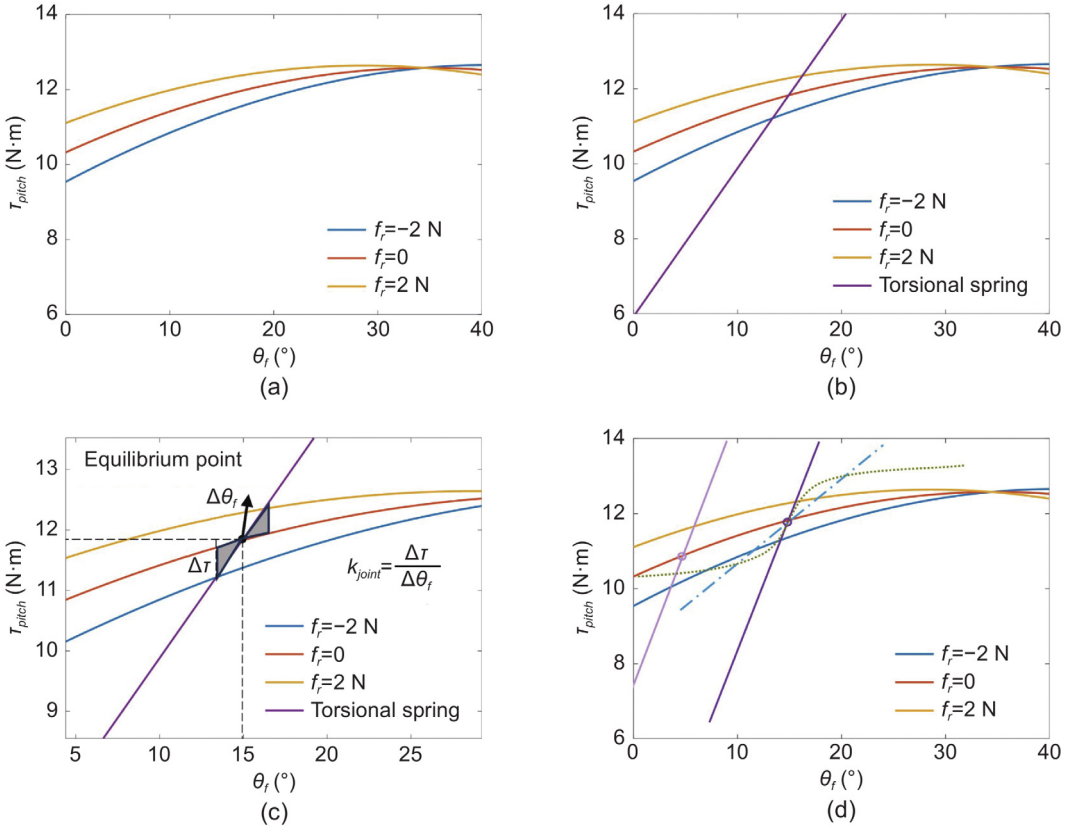

Fig. 10. Torque of pitch joint with respect to the pitch angle.

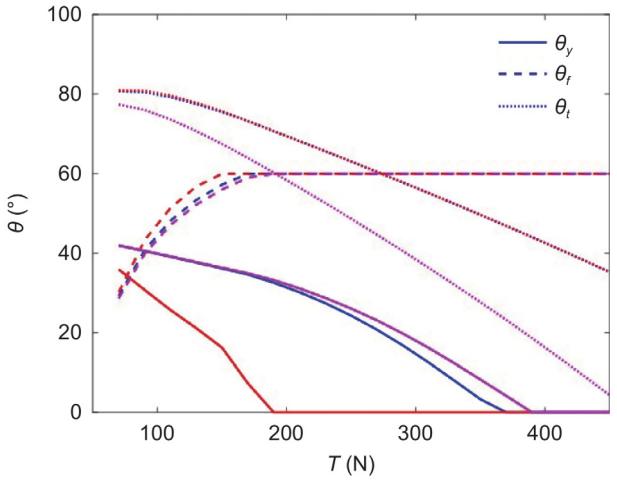

Fig. 11. Three joint angles versus tendon force with different parameter settings. Blue: reference. Red: larger offset from yaw axis. Pink: larger knee pulley radius.

4. Leg design

In this section, the mechanical design of the leg for manufacturing experimental prototypes is described.

As Fig. 13 shows, the leg model includes laser cut plates to form the links (hip, femur and tibia), 3D printed joint shafts, mounting bases for motor and leg, ankle, coupling and some other small parts, as well as purchased fasteners, springs, wire, wheel and motors. The leg and the pull motor (tendon actuator) are fixed on the robot body separately, which can be arbitrarily customized according to need. The knee pulley is mounted on the front side of the fold shaft. A metal wire is tied to a bolt on the tibia, then passed around the pulley, and the end will be tied to a wire reel on the shaft of pull motor.

The torsional springs for pitch and fold joints are mounted on their respective joint shafts, and their feet are resting on different links in front and behind them, so that joint torques are generated after deformation. These torsional springs also only work in one direction, and will be released when joint angle goes beyond the installation angle.

Local details of the hip are shown in Fig. 14. The “hip joint” in our leg is to combine femur and the chassis, and allows two orthogonal rotational DOFs (yaw and pitch). The shaft under the hip block (3) inserts into the shaft sleeve on hip base (5) to form yaw axis. The bolt between them is not fast tightened, so that hip can rotate about the yaw axis but not leave the sleeve.

Yaw springs are mounted on two cylinders on the hip base. One foot of the spring is anchored on the hip base and the other is stopped by cylinder on hip block. The yaw springs only work in one direction: When hip rotates clockwise, the right spring is compressed, and the left one is set free and stay at its initial position, vice versa. The previous mentioned stiffness of yaw torsional spring is therefore the stiffness of either spring. Theoretically, the two springs can be designed differently and have different stiffness, though we set them the same here. The spring force is not linearly dependent to the yaw angle, because their axis is not concentric with the rotation axis, in order to avoid conflict. This nonlinear does not affect its function much.

Pitch joint shaft will be installed through the holes on hip plates. The series of pre-made bolt holes (1.b) provide flexibility

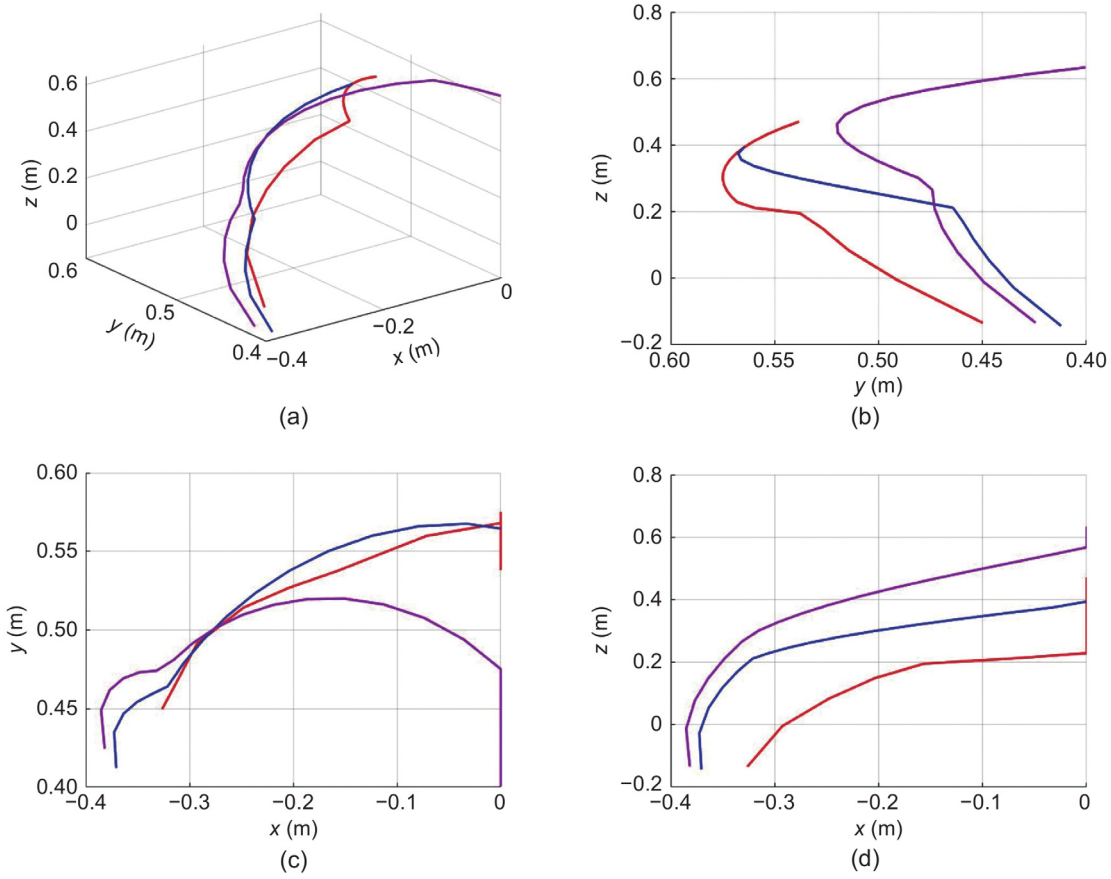

Fig. 12. The leg end trajectory in space with different parameter settings. Blue: reference. Red: larger offset from yaw axis. Pink: larger knee pulley radius. (a) 3D curve. (b) Left view. (c) Top view. (d) Rear view.

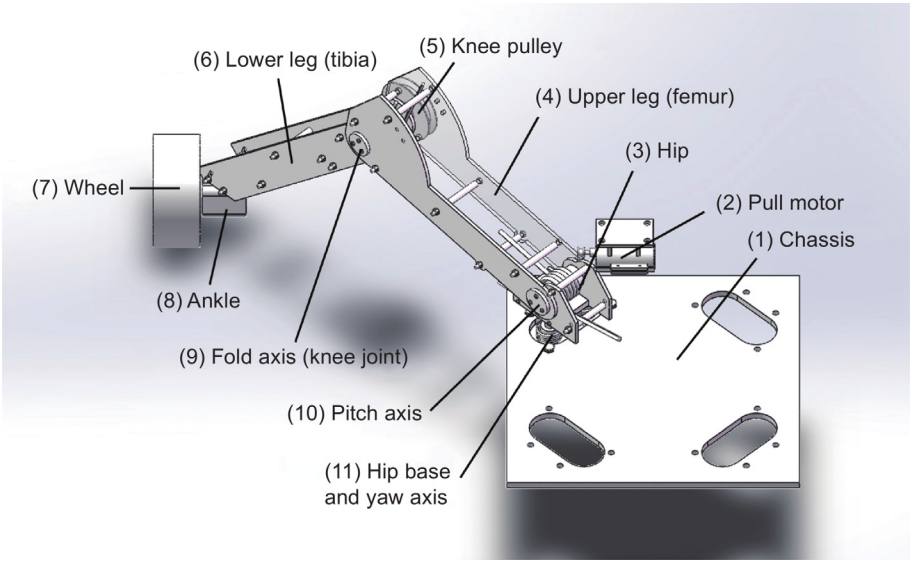

Fig. 13. Model of the leg with torsional springs.

for pitch spring installing and enable the adjustment of nominal configuration according to the payload or the environment. The bolts and sleeves (2) are to hold the two side plates parallel at a certain distance, and at the same time restrict the pitch joint angle in a certain range. This design is also applied to the femur and tibia.

5. Experiments

5.1. Experiments on the one-leg prototype

A preliminary one-leg prototype was built to evaluate the operating performance of the proposed leg mechanism. A load

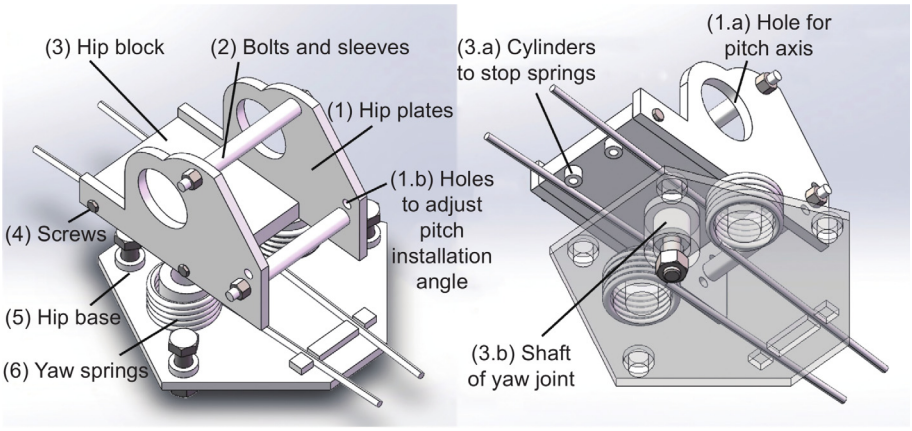

Fig. 14. Structure of the hip and yaw joint.

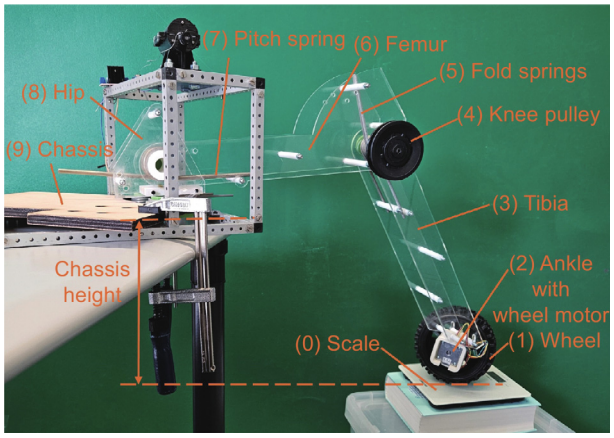

Fig. 15. Experimental setup to test the one-leg load capacity in standing state.

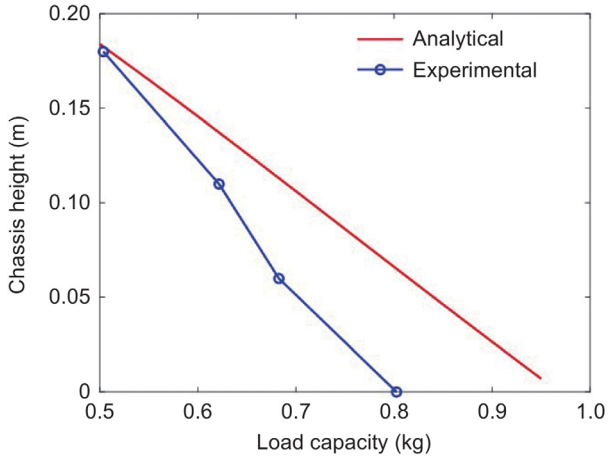

Fig. 16. Experimental and analytical load capacity versus floating chassis height.

capacity test in standing state and a leg-lifting experiment are conducted on the prototype. The main goal of the experiments is to test whether the leg configuration during the driving state as well as the end trajectory of the leg during the leg-lifting state conforms to the theoretical analysis in Section 3, and to check whether the system operates smoothly.

First, the various parts of the leg are manufactured or purchased separately and assembled. The main body of the leg links are made of laser cut acrylic boards. Joint shafts, ankle and some other components are 3D printed. Torsional springs are produced by Federntechnik Knoerzer GmbH. Wheel motor (Joy It stepper motor NEMA17-04) is also installed but not used in the experiments, since the one-leg prototype cannot drive independently.

In the load capacity test, the chassis is fixed on table by clamps, and the wheel stands on a scale, whose height is adjustable (Fig. 15). By measuring the contact force between the wheel and the "ground", we can infer the upward lifting force given by the leg to the vehicle chassis at the hip joint. The load capacity on a single leg at a certain chassis height is exactly the reading on the scale minus the mass of the leg below the hip joint (i.e. femur, tibia, ankle and wheel). The tendon is not tied to the leg at this experiment.

According to the analysis in Section 3, the load capacity of leg is related to the chassis height, or we should say the height of the floating chassis will automatically adapts to the actual load of the vehicle. Therefore, we measured the leg load capacity at different floating chassis heights and compared it with theoretical results (Fig. 16). We can see that the test results are generally in good agreement with the theoretical values. The load capacity near the preferred chassis height (around 0.18 m) is around 0.5 kg of one leg, and thus 2 kg of the whole vehicle. However, it can also be noticed that both curves are approximately straight lines, while in the experiment the floating chassis height drops faster than the theoretical value as the load increases. The main reason of this phenomenon is that the material property of the purchased springs contains non-linearity, which makes the springs behave weaker when compressed at larger angles. In addition, it should be noted that the spring installation angles selected under this load test condition are $\theta_{0f} = 0\,\text{deg}$ and $\theta_{0t} = 75\,\text{deg}$, which is a moderate setting to reduce the manufacturing difficulty of the leg prototype. If we choose larger spring installation angles such as $\theta_{0f} = -20\,\text{deg}$ and $\theta_{0t} = 80\,\text{deg}$, the theoretical load capacity of the leg and the robot could reach 1.47 kg and 5.88 kg, respectively.

In the leg-lifting experiment, the leg and motor are fixed respectively to a base board and a steel frame, and then clamped on the table together (Fig. 17 and Fig. 18). After that, the metal wire (tendon) is tied and electronic system is connected. An Arduino board (UNO R3) is used to receive command from computer and send control PWM (pulse-width modulation) signal to the motor driver. The motor driver (L298N) provides power to the pull motor, and controls motor output according to received PWM signal. In this way, the maximum pull torque of the DC geared motor (Modelcraft RB350050-22723R) can be controlled by PC command.

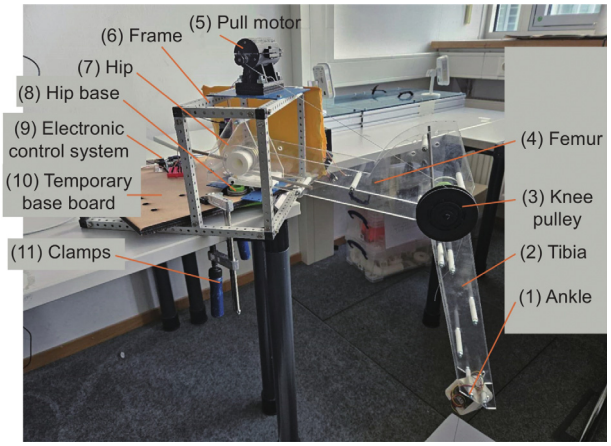

Fig. 17. Experiment setup for the leg-lifting test.

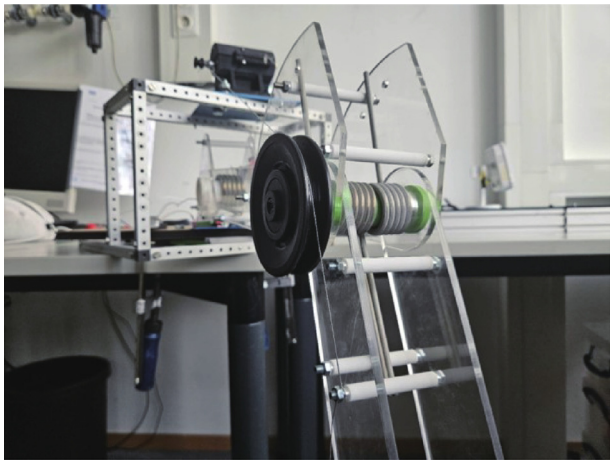

Fig. 18. Close-up of the leg-lifting mechanism, including knee joint, fold springs, knee pulley, pull motor and metal wire as tendon.

Table 1
Measured parameter of the leg prototype.

Parameter	Value	Parameter	Value
l_f	0.350 m	m_f	0.7858 kg
l_t	0.400 m	m_t	0.4306 kg
c_f	0.791	m_w	0.3371 kg
c_t	0.498	$m_{pull\ motor}$	0.4574 kg
k_{yaw}	0.055 N·m/deg	θ_{0yaw}	40 deg
k_{pitch}	0.395 N·m/deg	θ_{0f}	−10 deg
k_{fold}	0.266 N·m/deg	θ_{0t}	70 deg
x_p	0.025 m	R_k	0.035 m
y_p	0.035 m	S_k	0.06 m
z_p	0.165 m		

The structural parameters of the one-leg prototype in the leg-lifting experiment are shown in Table 1. Total leg mass weighs 2.4 kg including all leg components, pull motor and its base, wheel and wheel motor. Stiffness of springs are given by manufacturer and not actually measured. To draw the end trajectory, we increase the duty cycle of PWM step by step, and run the motor for a short time at each command until the leg no longer move. In this way, a certain leg end position is associated with a certain duty cycle value, which also indicates a certain motor torque and the tendon pulling force. At each duty cycle step, the coordinates of the leg end are measured manually with a ruler with the help of a plumb line. As the pulling force increases step by step, the leg is gradually lifted upwards, and an end trajectory is drawn.

Experimental and theoretically calculated end trajectories are compared in Fig. 19 (video clips showing the experimental process also accompany this article). The coordinate origin is the intersection point of yaw and pitch axis, which can be regarded as the center of hip. Overall, the trend of the experimental endpoint trajectory is consistent with the theoretical curve. However, it can also be noticed that the experimental curve is generally lower than the theoretical curve, and in the later part, the growth of the x-coordinate slows down, while the y-coordinate grows more. The possible reason for this difference is that the joint friction in the prototype is large. This hinders the leg from being raised smoothly and counteract the effect of tendon force. On the other hand, although the femur is not lifted as it should due to the friction force, the sufficient tendon force still works on the tibia and stretches the knee joint. Hence, the leg sticks further forward and the y-coordinate (forward driving direction) seems to be larger relative to its z-coordinate (height). To address this issue, bearings could be introduced in future work to reduce the joint friction in the leg prototype.

The endpoint of the leg is lifted by 25 cm during the preliminary experiment, which is around 1.3 times the corresponding chassis height in such parameter setting. As a comparison, "Complios" can cross a trapezoidal obstacle of 15 cm (0.44 times its nominal height) [26], "Epi.q-1" can overcome 9 cm steps (0.72 of the height of its locomotion unit) [27] and "Spot" has the maximum step height of 30 cm (around 0.6 times its chassis height). If we take into account the gap between the experimental and theoretical values under the influence of friction, we can assume that the leg-lifting performance will be better than this with optimized mechanism design.

5.2. Experiments on the four-legged robot platform

In order to evaluate the performance of the wheeled legs in the robot's passive and active obstacle-crossing modes, we fabricated a four-legged spider-inspired robot platform. With different spring installation angles, the robot can achieve various nominal configurations (Fig. 20). This robot prototype is equipped with four stepper motors (Joy It NEMA17-04) to drive the wheels, and two geared DC motors (Modelcraft RB350050-22723R) to pull the tendons for the front legs. The corresponding motor drivers are STEPPERONLINE DM320T and L298N respectively. The robot's movement is also controlled by the Arduino UNO board and powered by an external power supply.

In the locomotion experiments, we set the running speed of the spider-inspired robot as 1 m/s. The robot prototype can passively cross obstacles with a slope of 17 deg and a maximum height of 11 cm (Fig. 21). With the help of active tendon pulling, its obstacle-climbing ability is improved and it can actively cross obstacles with a slope of 25 deg and a maximum height of 15.5 cm (see the supplementary video accompanying this article).

In summary, the locomotion experiments showed that the leg and robot prototype performed as expected and consistent with theory. Since our current prototype is only a preliminary model, this performance could still be improved, e.g., by performing structural optimization on the compliant mechanism or by adding a reducer to the wheel motor to provide larger torque for the wheel.

6. Discussion and conclusion

In this paper, a spider-inspired semi-tendon-driven compliant wheeled leg is proposed for quadruped search mobile robots.

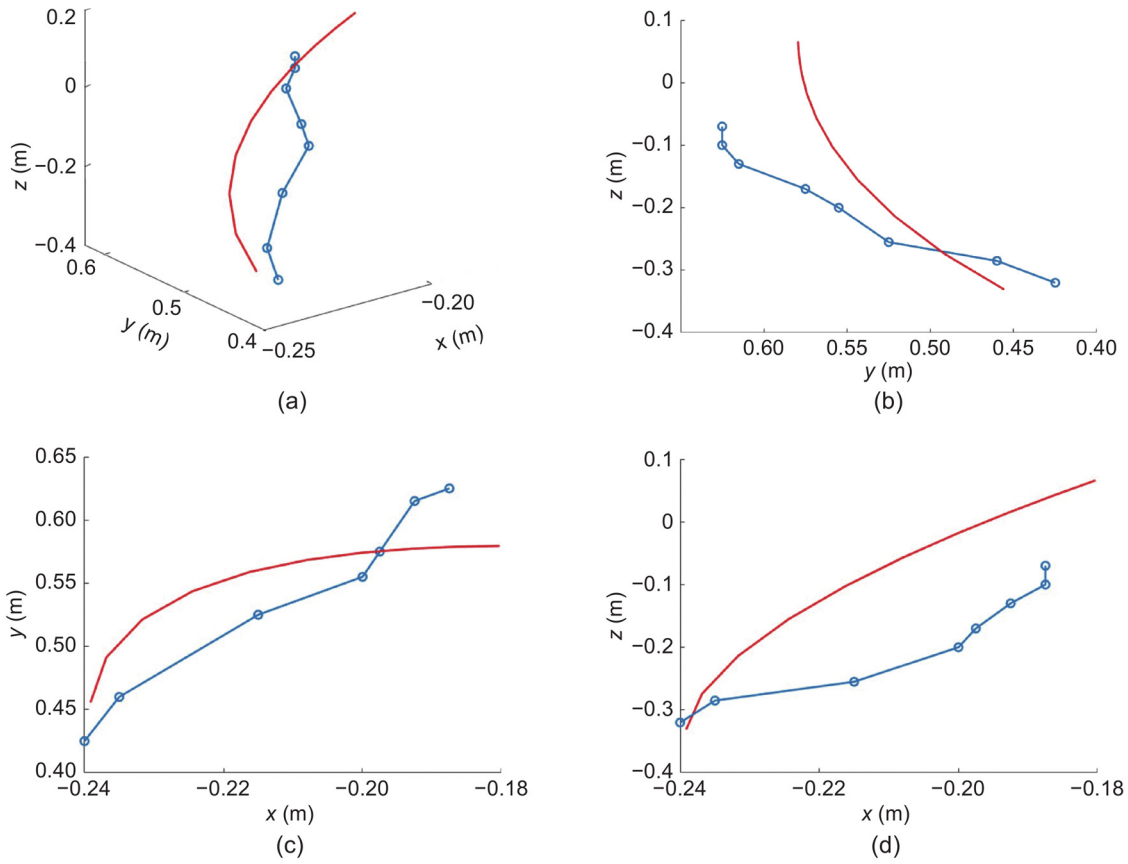

Fig. 19. Endpoint trajectories of the experiment and theoretically calculated results. (a) - (d) show different views of the trajectories. Dotted blue curve: experimental results; Smooth red curve: theoretically calculated results. (a) 3D curve. (b) Left view. (c) Top view. (d) Rear view.

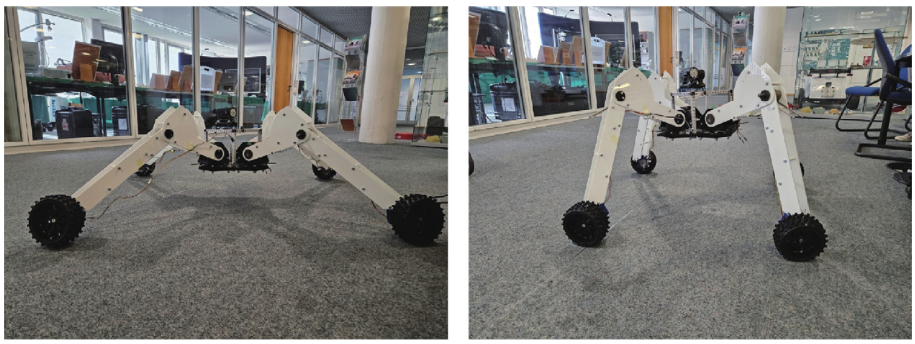

Fig. 20. Side view of the robot platform with different springs installation angles. (a) Lower configuration with $\theta_{0t} = 90\,deg$, (b) Higher configuration with $\theta_{0t} = 135\,deg$.

The created robot leg has four motion DOFs in total: three DOFs in the leg configuration with semi-tendon-driven actuation and one DOF in the drive wheel with direct motor actuation. This compliant leg allows search robot to adapt well to irregular terrain and travel at a considerable speed like an off-road vehicle with low control costs. The four legs of the robot are distributed diagonally and the upper legs are above the chassis, so that the robot can resist rollover during locomotion. In addition, the realized robot platform also has adjustable chassis height and wheel track.

Different from the traditional fully-actuated method with independent motor joint control, the proposed leg utilizes a simplified semi-tendon-driven mechanism with compliant joints for obstacle-crossing. In addition to the passive adaptation mode, this design also allows the realized robot platform to lift the 3-DOF leg with a single tendon to actively adapt itself to higher obstacles.

Experiments on a one-leg prototype and a robot platform were also performed. Results showed that the load capacity in the driving state of one leg can vary from 0.5 kg to 1.5 kg, depending on springs installation angles. As for the preliminary leg-lifting experiment, the robot leg was raised by 0.25 m, which is 1.3 times of its chassis height. This result outperforms the robots in [26,27], which can generally cross obstacles lower than the chassis without jumping. In the robot platform experiment, the leg can passively overcome obstacles with a height of 11 mm and actively overcome obstacles with a height of 15.5 mm at a speed

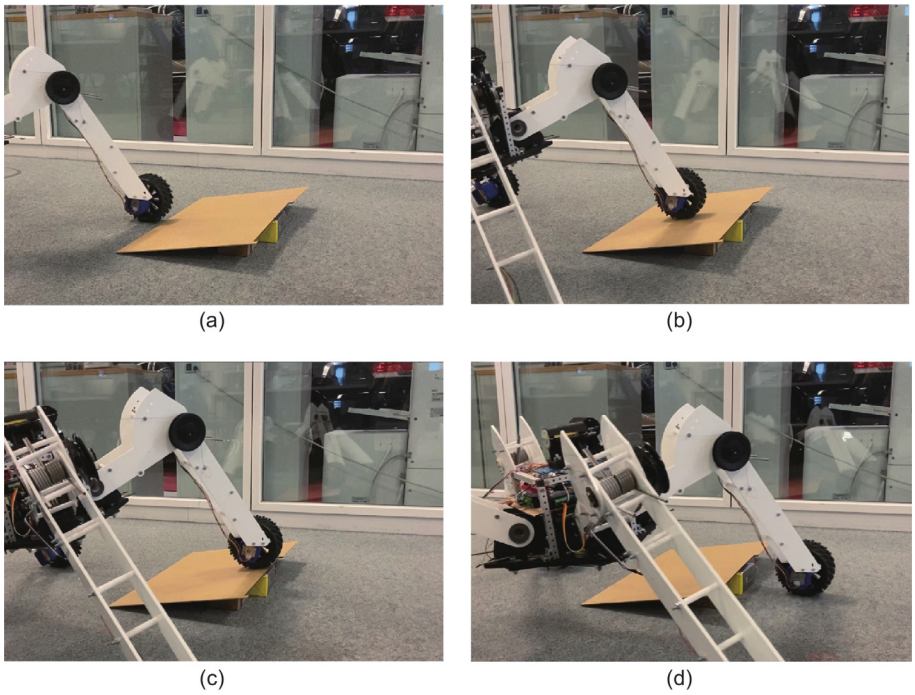

Fig. 21. One leg of the four-legged robot platform climb over an obstacle (11 cm height) in the passive adaptation mode. (a) Leg in nominal configuration before encountering obstacle. (b) - (c) Leg was compressed by the obstacle and self-adapted to overcome it. (d) Leg passed the obstacle.

of 1 m/s. Since our robot platform was only a preliminary model, this locomotion performance can still be improved.

The tendon-driven design presented in this work also reduced the requirements on the pull motor due to the amplification by moment arm. Under the experimental parameter setting, if friction is not considered, the pull motor shaft only needs to provide a torque of about 0.15 N·m to raise the leg end above the chassis. For comparison, the required pitch joint torque at this time is about 28 N·m.

Overall, this work provided a novel design concept of compliant locomotion system for obstacle-crossing or exploration mobile robots, established the model and theory of the "spider-like" type of wheeled robot leg, implemented a MATLAB program for design assistance, and carried out preliminary experimental tests for evaluation of the leg performance.

Nevertheless, there is still a lot of work to be done, and the leg design leaves a lot to be improved. For example, bearings should be added to reduce the joint friction and the introduce of motor reducers will help to provide larger torque for wheels. In addition, four-leg coordination should be considered and improved on the robot platform. Furthermore, the design potential of compliant joints or links should be further explored. And for practical reasons, life-cycle tests of battery and compliant components should also be carried out.

CRediT authorship contribution statement

Yilin Wang: Writing – original draft, Validation, Software, Methodology, Investigation, Formal analysis. **Felix Pancheri:** Resources. **Tim C. Lueth:** Funding acquisition. **Yilun Sun:** Writing – review & editing, Supervision, Project administration, Conceptualization.

Declaration of competing interest

The authors declare that they have no known competing financial interests or personal relationships that could have appeared to influence the work reported in this paper.

Acknowledgments

This research is supported by the teaching funding of TUM School of Engineering and Design.

Appendix A. Supplementary data

Supplementary material related to this article can be found online at https://doi.org/10.1016/j.birob.2024.100182.

References

[1] A.G. Macintyre, J.A. Barbera, E.R. Smith, Surviving collapsed structure entrapment after earthquakes: a "time-to-rescue" analysis, Prehospital Disaster Med. 21 (1) (2006) 4–17.
[2] A.G. Macintyre, J.A. Barbera, B.P. Petinaux, Survival interval in earthquake entrapments: research findings reinforced during the 2010 haiti earthquake response, Disaster Med. Public Health Prep. 5 (1) (2011) 13–22.
[3] J. Delmerico, S. Mintchev, A. Giusti, B. Gromov, K. Melo, T. Horvat, C. Cadena, M. Hutter, A. Ijspeert, D. Floreano, et al., The current state and future outlook of rescue robotics, J. Field Robotics 36 (7) (2019) 1171–1191.
[4] F. Li, S. Hou, C. Bu, B. Qu, Rescue robots for the urban earthquake environment, Disaster Med. Public Health Prep. 17 (2023) e181.
[5] T.M. Dawdi, N. Abdalla, Y.M. Elkalyoubi, B. Soudan, Locating victims in hot environments using combined thermal and optical imaging, Comput. Electr. Eng. 85 (2020) 106697.
[6] K. Sharma, R. Doriya, S.K. Pandey, A. Kumar, G. Sinha, P. Dadheech, Real-time survivor detection system in SaR missions using robots, Drones 6 (8) (2022) 219.
[7] N. Michael, S. Shen, K. Mohta, V. Kumar, K. Nagatani, Y. Okada, S. Kiribayashi, K. Otake, K. Yoshida, K. Ohno, et al., Collaborative mapping of an earthquake damaged building via ground and aerial robots, in: Field and Service Robotics: Results of the 8th International Conference, Springer, 2014, pp. 33–47.
[8] E. Rohmer, K. Ohno, T. Yoshida, K. Nagatani, E. Konayagi, S. Tadokoro, Integration of a sub-crawlers' autonomous control in quince highly mobile rescue robot, in: 2010 IEEE/SICE International Symposium on System Integration, IEEE, 2010, pp. 78–83.
[9] E. Rohmer, T. Yoshida, K. Ohno, K. Nagatani, S. Tadokoro, E. Konayagi, Quince: A collaborative mobile robotic platform for rescue robots research and development, in: The Abstracts of the International Conference on Advanced Mechatronics: Toward Evolutionary Fusion of IT and Mechatronics: ICAM 2010.5, The Japan Society of Mechanical Engineers, 2010, pp. 225–230.

[10] M. Raibert, K. Blankespoor, G. Nelson, R. Playter, Bigdog, the rough-terrain quadruped robot, IFAC Proc. Vol. 41 (2) (2008) 10822–10825.
[11] S. Zimmermann, R. Poranne, S. Coros, Go fetch!-dynamic grasps using boston dynamics spot with external robotic arm, in: 2021 IEEE International Conference on Robotics and Automation, ICRA, IEEE, 2021, pp. 4488–4494.
[12] Y. Sun, Z. Wang, F. Pancheri, T.C. Lueth, Toqro: A flexible quadruped walking robot with topology optimized soft legs, in: 2024 IEEE 7th International Conference on Soft Robotics (RoboSoft), IEEE, 2024, pp. 61–66.
[13] Y. Sun, F. Pancheri, C. Rehekampff, T.C. Lueth, TurBot: A turtle-inspired quadruped robot using topology optimized soft-rigid hybrid legs, IEEE/ASME Trans. Mechatronics 29 (4) (2024) 3193–3202.
[14] Y. Sun, C. Zong, F. Pancheri, T. Chen, T.C. Lueth, Design of topology optimized compliant legs for bio-inspired quadruped robots, Sci. Rep. 13 (2023) 4875.
[15] S. Hirose, A. Morishima, Design and control of a mobile robot with an articulated body, Int. J. Robotics Res. 9 (2) (1990) 99–114.
[16] C. Wright, A. Buchan, B. Brown, J. Geist, M. Schwerin, D. Rollinson, M. Tesch, H. Choset, Design and architecture of the unified modular snake robot, in: 2012 IEEE International Conference on Robotics and Automation, IEEE, 2012, pp. 4347–4354.
[17] J. Whitman, N. Zevallos, M. Travers, H. Choset, Snake robot urban search after the 2017 mexico city earthquake, in: 2018 IEEE International Symposium on Safety, Security, and Rescue Robotics, SSRR, IEEE, 2018, pp. 1–6.
[18] Y. Di, Y. Zhang, Y. Wen, H. Yao, Z. Zhou, Z. Ren, H. Tian, J. Shao, Inchworm-inspired soft robot with controllable locomotion based on self-sensing of deformation, IEEE Robot. Autom. Lett. (2024).
[19] Y. Peng, H. Nabae, Y. Funabora, K. Suzumori, Controlling a peristaltic robot inspired by inchworms, Biomim. Intell. Robotics 4 (1) (2024) 100146.
[20] Y. Peng, H. Nabae, Y. Funabora, K. Suzumori, Peristaltic transporting device inspired by large intestine structure, Sensors Actuators A 365 (2024) 114840.
[21] C. Grand, F. BenAmar, F. Plumet, P. Bidaud, Decoupled control of posture and trajectory of the hybrid wheel-legged robot hylos, in: IEEE International Conference on Robotics and Automation, 2004. Proceedings. ICRA'04. 2004, Vol. 5, IEEE, 2004, pp. 5111–5116.
[22] C. Grand, F. Benamar, F. Plumet, P. Bidaud, Stability and traction optimization of a reconfigurable wheel-legged robot, Int. J. Robotics Res. 23 (10–11) (2004) 1041–1058.
[23] C. Grand, F. Benamar, F. Plumet, Motion kinematics analysis of wheeled–legged rover over 3D surface with posture adaptation, Mech. Mach. Theory 45 (3) (2010) 477–495.
[24] C. Grand, P. Jarrault, F.B. Amar, P. Bidaud, Experimental evaluation of obstacle clearance by a hybrid wheel-legged robot, in: Experimental Robotics: The 14th International Symposium on Experimental Robotics, Springer, 2016, pp. 47–58.
[25] A. Bouton, C. Grand, F. Benamar, Obstacle negotiation learning for a compliant wheel-on-leg robot, in: 2017 IEEE International Conference on Robotics and Automation, ICRA, IEEE, 2017, pp. 2420–2425.
[26] A. Bouton, C. Grand, F. Benamar, Design and control of a compliant wheel-on-leg rover which conforms to uneven terrain, IEEE/ASME Trans. Mechatronics 25 (5) (2020) 2354–2363.
[27] G. Quaglia, D. Maffiodo, W. Franco, S. Appendino, R. Oderio, The epi. q-1 hybrid mobile robot, Int. J. Robotics Res. 29 (1) (2010) 81–91.
[28] M. Bjelonic, C.D. Bellicoso, Y. de Viragh, D. Sako, F.D. Tresoldi, F. Jenelten, M. Hutter, Keep rollin'—whole-body motion control and planning for wheeled quadrupedal robots, IEEE Robot. Autom. Lett. 4 (2) (2019) 2116–2123.
[29] Z. Chen, J. Li, J. Wang, S. Wang, J. Zhao, J. Li, Towards hybrid gait obstacle avoidance for a six wheel-legged robot with payload transportation, J. Intell. Robot. Syst. 102 (3) (2021) 60.
[30] S.-C. Chen, K.-J. Huang, W.-H. Chen, S.-Y. Shen, C.-H. Li, P.-C. Lin, Quattroped: a leg–wheel transformable robot, IEEE/ASME Trans. Mechatronics 19 (2) (2013) 730–742.
[31] Y.-S. Kim, G.-P. Jung, H. Kim, K.-J. Cho, C.-N. Chu, Wheel transformer: A wheel-leg hybrid robot with passive transformable wheels, IEEE Trans. Robot. 30 (6) (2014) 1487–1498.
[32] S.-S. Yun, J.-Y. Lee, G.-P. Jung, K.-J. Cho, Development of a transformable wheel actuated by soft pneumatic actuators, Int. J. Control Autom. Syst. 15 (1) (2017) 36–44.
[33] H. Chai, Y. Li, R. Song, G. Zhang, Q. Zhang, S. Liu, J. Hou, Y. Xin, M. Yuan, G. Zhang, et al., A survey of the development of quadruped robots: Joint configuration, dynamic locomotion control method and mobile manipulation approach, Biomim. Intell. Robotics 2 (1) (2022) 100029.
[34] H. Taheri, N. Mozayani, A study on quadruped mobile robots, Mech. Mach. Theory 190 (2023) 105448.
[35] D. Qin, G. Zhang, Z. Zhu, X. Zeng, J. Cao, An online terrain classification framework for legged robots based on acoustic signals, Biomim. Intell. Robotics 3 (2) (2023) 100091.
[36] Y. Zhang, J. Zhang, B. Chen, H. Chen, A. Song, Obstacle detection and autonomous stair climbing of a miniature jumping robot, Biomim. Intell. Robotics 3 (1) (2023) 100085.
[37] C. Zhang, J. Chen, J. Li, Y. Peng, Z. Mao, Large language models for human-robot interaction: A review, Biomim. Intell. Robotics 3 (4) (2023) 100131.
[38] Y. Sun, T.C. Lueth, Enhancing torsional stiffness of continuum robots using 3-D topology optimized flexure joints, IEEE/ASME Trans. Mechatronics 28 (4) (2023) 1844–1852.
[39] Y. Sun, Y. Liu, F. Pancheri, T.C. Lueth, LARG: A lightweight robotic gripper with 3-D topology optimized adaptive fingers, IEEE/ASME Trans. Mechatronics 27 (4) (2022) 2026–2034.
[40] H. Surmann, K. Daun, M. Schnaubelt, O. von Stryk, M. Patchou, S. Böcker, C. Wietfeld, J. Quenzel, D. Schleich, S. Behnke, et al., Lessons from robot-assisted disaster response deployments by the German rescue robotics center task force, J. Field Robotics (2023).
[41] R. Ozawa, H. Kobayashi, K. Hashirii, Analysis, classification, and design of tendon-driven mechanisms, IEEE Trans. Robotics 30 (2) (2013) 396–410.